Ion transfer and adsorption of water-soluble metal complexes of 8-hydroxyquinoline derivatives at the water|1,2-dichloroethane interface

Ion transfer and adsorption of water-soluble metal complexes of 8-hydroxyquinoline derivatives at the water|1,2-dichloroethane Interface

Sho Yamamoto [a], Shohei Kanai [a], Marie Takeyama [b], Yoshio Nishiyama [c], Hisanori Imura [c], and Hirohisa Nagatani [c,*]

[a]Division of Material Chemistry, Graduate School of Natural Science and Technology, Kanazawa University, Kakuma, Kanazawa 920-1192, Japan

[b]School of Chemistry, College of Science and Engineering, Kanazawa University, Kakuma, Kanazawa 920-1192, Japan

[c]Faculty of Chemistry, Institute of Science and Engineering, Kanazawa University, Kakuma, Kanazawa 920-1192, Japan

*To whom correspondence should be addressed: H. Nagatani

E-mail: nagatani@se.kanazawa-u.ac.jp

ABSTRACT

The transfer mechanism and adsorption state of water-soluble 8-quinolinolate complexes were studied at the water|1,2-dichloroethane interface by electrochemical and spectroelectrochemical techniques. The interfacial affinities of the metal complexes of 8-hydroxyquinoline-5-sulfonate (QS) were estimated as $Al(QS)_3^{3-}$, $Cu(QS)_2^{2-}$ > $Zn(QS)_2^{2-}$. Potential modulated fluorescence spectroscopy revealed the potential-driven process of fluorescent QS complexes, where Al(III) and Zn(II) complexes were transferred across the interface accompanied by the adsorption at the aqueous side of the interface. The adsorption state and preferential molecular orientation of these complexes were analyzed in detail by polarization-modulation total internal reflection fluorescence (PM-TIRF) spectroscopy. The PM-TIRF results showed that the square-planar 1:2 complexes, $Al(QS)_2^-$ and $Zn(QS)_2^{2-}$, were oriented relatively in parallel to the interface and approximately identical to the aqueous species. The adsorption behavior of the Zn(II) complex of tridentate 8-hydroxyquinoline-2-carboxylate (QC) ligand was also investigated, and $Zn(QC)_2^{2-}$ exhibited a strong interfacial affinity with intermediate spectral features between the aqueous and organic species.

1. Introduction

The interfacial region between two immiscible solutions is a two-dimensional reaction field with a thickness of a few nm, where the physicochemical parameters such as density, polarity and electric potential etc., are significantly modified from those of the adjacent bulk phases [1, 2]. The interfacial reactivity of charged species is often influenced by specific hydration/solvation and dynamics in the interfacial region. The interfacial mechanism has been studied by a variety of surface-sensitive spectroscopy and electrochemical approach [3-5]. The ionic partitioning and charge transfer reactions at the interface can be driven as a function of the Galvani potential difference between two phases ($\Delta_o^w \phi$). Therefore, the electrochemical approach such as ion transfer voltammetry is a useful method to analyze the interfacial mechanism of charged species [6-8]. The spectroelectrochemical technique uncover further detail of the interfacial mechanism by combining the quantitative electrochemical control of charge transfer reaction and highly-selective spectroscopic characterization of interfacial species. The fluorescence-based techniques, such as potential-modulated fluorescence (PMF) [9, 10] and polarization-modulation total internal reflection fluorescence (PM-TIRF) techniques [11], have advantages with respect to sensitive analysis of potential-driven dynamic behavior and *in situ* characterization of interfacial species, respectively. In these techniques, the undesirable charge transfer of nonfluorescent species is entirely negligible, and the sensitive detection of target fluorescent species is readily conducted by selecting the excitation and emission wavelengths. PM-TIRF spectroscopy, for instance, elucidated the potential-induced aggregation mechanism of anionic porphyrins at liquid|liquid interfaces through selective detection of interfacially formed J-aggregates [12].

8-Hydroxyquinoline (HQ) and its derivatives are widely-used chelating agents for spectrophotometric determination of various metal ions [13]. Aluminum(III), magnesium(II) and

zinc(II) quinolinolato complexes, particularly, show pronounced fluorescence properties although a free ligand emits weak fluorescence. The metal quinolinolato complexes have also been functionalized in organic light emitting devices [14, 15]. In terms of separation chemistry, the facilitated ion transfer (electrochemical solvent extraction) of metal ions by the lipophilic HQ has been studied at liquid|liquid interfaces under electrochemical control, where a slight partitioning of ligands into the aqueous phase occurs, accompanied by the complexation homogeneously, and finally, the metal complexes are transferred into the organic phase [16-19]. The selective transfer of metal complex with hydrophilic ligands into the organic phase can also be achieved by applying an appropriate Galvani potential difference. It is known that the liquid-liquid partitioning of metal complexes is affected by pH (hydrolysis of metal ion and protonation of ligand), concentrations of metal ion and ligand, net charges, and so on. The complicated heterogeneous mechanism of metal complexes including ion transfer and adsorption processes, thus, has rarely been studied in detail [20, 21].

In the present study, the adsorption behavior of water-soluble 8-quinolinolato complexes with Al(III), Cu(II), and Zn(II) was examined at the polarized water|1,2-dichloroethane (DCE) interface. The interfacial mechanism of fluorescent complexes with Al(III) and Zn(II) were characterized in detail by PMF and PM-TIRF techniques. The effect of molecular geometry on the interfacial behavior was also investigated by employing bi- and tridentate ligands.

2. Experimental

2.1. Electrochemical cell

8-Hydroxyquinoline-5-sulfonic acid (H_2QS), monohydrate (TCI, EP, >98.0%) and 8-hydroxyquinoline-2-carboxylic acid (H_2QC) (Aldrich, ≥98.0%) were used as received. The

aqueous solutions of metal complexes were prepared by dissolving appropriate amounts of chelating ligand and metal chloride, aluminum(III) chloride (Sigma-Aldrich, 98%), zinc(II) chloride (Nacalai Tesque, GR, ≥98%), and copper(II) chloride dihydrate (Wako, ≥99%). The purified water by a Milli-Q system (Millipore, Direct-Q3UV) and DCE (Nacalai Tesque, HPLC grade, ≥99.7%) were saturated with each other and used for solution preparation. The compositions of the electrochemical cells are represented in **Figure 1**. The supporting electrolytes were 1.0×10^{-2} mol dm^{-3} LiCl (**Cell I**) or Li_2SO_4 (**Cell II**) for the aqueous phase and 5.0×10^{-3} mol dm^{-3} bis(triphenylphosphoranylidene)ammonium tetrakis(pentafluorophenyl)borate (BTPPATPFB) for the organic phase, respectively. BTPPATPFB was prepared by metathesis of bis(triphenylphosphoranylidene)ammonium chloride (BTPPACl) (Aldrich, 97%) and lithium tetrakis(pentafluorophenyl)borate ethyl ether complex (TCI, > 70%). All other reagents were of analytical grade or higher. The pH condition was adjusted by the addition of HCl (**Cell I**), H_2SO_4 (**Cell II**), LiH_2PO_4/LiOH buffer or H_3BO_3/LiOH buffer.

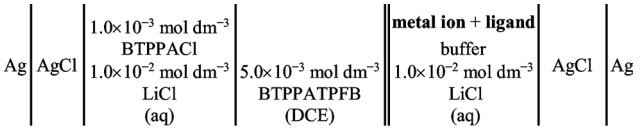

(Cell I)

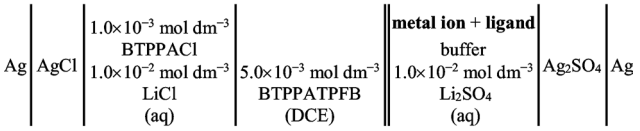

(Cell II)

Figure 1. Schematic representation of the electrochemical cells.

2.2. Spectroelectrochemical analysis

The spectroelectrochemical cell was analogous to one reported previously [10]. The water|DCE interface with an interfacial area of 0.50 cm^2 was polarized by a four-electrode

potentiostat (Hokuto Denko, HA-1010mM1A). The Galvani potential difference ($\Delta_o^w\phi \equiv \phi^w - \phi^o$) was estimated by taking the formal transfer potential ($\Delta_o^w\phi^{o'}$) of tetramethylammonium ions as 0.160 V [22]. All experiments were carried out in a thermostated room at 298±2 K. The water|DCE interface was illuminated in total internal reflection (TIR) from the organic phase by a cw laser diode either at 404 nm (Coherent, CUBE 405-50C) or at 376 nm (Coherent, OBIS 375LX-50). The angle of incidence (ψ_i) was ca. 75°. A Fresnel rhomb half-wave plate (Sigma Koki) was placed to select the linear polarization angle of the excitation beam. The fluorescence signal from the interfacial region was measured perpendicularly to the interface by an optical fiber and a monochromator equipped with a photomultiplier tube (Shimadzu, SPG-120S).

The PMF study was carried out by analyzing the fluorescence signal from the interfacial region as a function of ac potential modulation. The PMF signal was analyzed by a digital lock-in amplifier (NF LI5640) for dc-potential sweep mode, while a frequency response analyzer (NF FRA5022) was employed for frequency dependence analysis at a given $\Delta_o^w\phi_{dc}$. Details of the analytical procedure are described elsewhere [9].

In the PM-TIRF experiment, the linear polarization of an excitation beam was periodically modulated between p- (parallel to the plane of incidence) and s-polarizations (perpendicular to the plane of incidence) at 13 Hz by a liquid crystal retarder (LCR) (Thorlabs, LCC1111T-A or LCC25/TC200) [11, 12]. The polarization modulation efficiencies (P_m) of LCR, i.e., the fraction of the p- or s-polarized component in the excitation beam under respective light modulations, were obtained as 0.95 at 404 nm and 0.85 at 376 nm, respectively, indicating that 5 % and 15 % of the s-polarized component remain in the p-polarized mode of LCR or *vice versa*. The PM-TIRF signal ($\Delta F^{p\text{-}s}$) is defined as

$$\Delta F^{p\text{-}s} = F_m^p - F_m^s = (2P_m - 1)(F^p - F^s) \quad (1)$$

where F_m^p and F_m^s are the modulated fluorescence intensities measured with p- and s-polarized excitation modes, F^p and F^s are the fluorescence intensities arisen from the species oriented at the interface under p- and s-polarized excitations, respectively. The modulated fluorescence signal from the interfacial region was analyzed by a digital lock-in amplifier (NF, LI5640) as a function of periodic polarization modulation of the incident beam.

3. Results and discussion

3.1. Ionic partitioning and Adsorption behavior of QS species

The interfacial behavior of QS species was analyzed by electrochemical and spectroelectrochemical techniques. The charged state of the QS ligand and its ion transfer feature at the water|DCE interface are highly dependent on the pH condition. The ionic partition diagram of QS in **Figure 2** was obtained by analyzing the voltammetric data based on the transfer mechanism consisting of acid-base equilibria in the aqueous phase, ion transfer processes, and partition of neutral species (see Supplementary material: **S1**) [23-25]. The electrochemical analysis indicated that the transferring charged species across the water|DCE interface was the monoanionic HQS^- with $\Delta_o^w\phi^{\circ\prime}_{HQS^-} = -0.277\pm0.003$ V at 3 < pH < 9.5 (Supplementary material: **Figure S1**). The partition coefficient ($\log P_{H_2QS}$) of the neutral H_2QS was determined as $\log P_{H_2QS} = 0.05$ by taking literature values of $pK_{a1} = 4.09$ and $pK_{a2} = 8.66$ [26]. Under the present experimental conditions, the quantitative complexation of metal ions with QS ligands occur in the aqueous solution because of the high stability of their complexes. The formation constants (β_n) are $\log\beta_{1,Al} = 8.95$, $\log\beta_{2,Al} = 17.43$, $\log\beta_{3,Al} = 24.58$ for Al(III) complexes [27], $\log\beta_{1,Zn} = 7.54$, $\log\beta_{2,Zn} = 14.32$ for Zn(II) complexes [28], and $\log\beta_{1,Cu} = 12.50$, $\log\beta_{2,Cu} = 23.10$ for Cu(II) complexes [29], respectively. As described in Supplementary material: **S2**, the dominant species are, respectively, $Al(QS)_3^{3-}$,

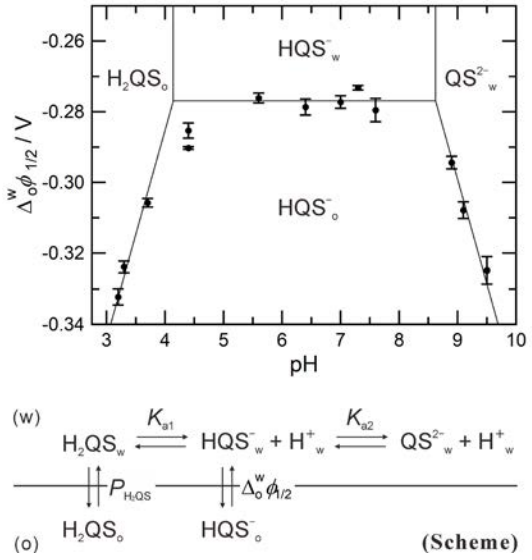

Figure 2. Ionic partition diagram for QS species across the water|DCE interface. The concentration of total QS species was 1.0×10^{-4} mol dm^{-3}. The solid boundary lines were obtained from the mechanistic analysis described in Supplementary material: **S1**. The subscripts w and o indicate the aqueous and organic species, respectively.

$Zn(QS)_2^{2-}$ and $Cu(QS)_2^{2-}$ at pH > 7, where no clear current peak for the ion transfer across the interface was observed within the potential window of cyclic voltammograms (CVs) even at the formal transfer potential of HQS^- (Supplementary material: **S3**). **Figure 3** shows the capacitance curves of the QS complexes measured at the water|DCE interface. The capacitance was increased at $\Delta_o^w\phi < -0.10$ V for each QS complex by the adsorption of negatively-charged species. Considering the charge on the complexes, their interfacial affinities around at –0.15 V were estimated as $Al(QS)_3^{3-} \approx Cu(QS)_2^{2-} > Zn(QS)_2^{2-}$. In the $Zn(QS)_2^{2-}$ system, the zinc(II) center coordinated with water molecules in the axial position [30-32] and it could lead to the enhancement of the hydrophilicity of $Zn(QS)_2^{2-}$, i.e., low interfacial affinity. On the other hand, the metal centers are hardly hydrated in the $Al(QS)_3^{3-}$ and $Cu(QS)_2^{2-}$ systems.

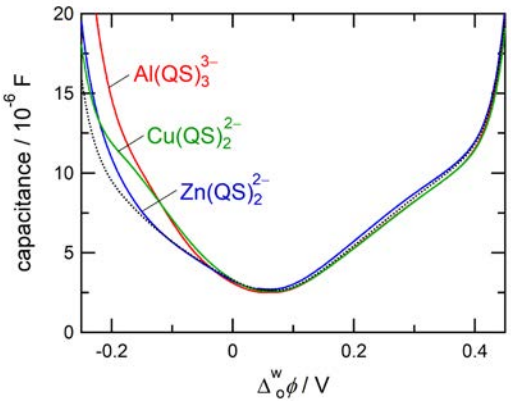

Figure 3. Capacitance curves measured for $Al(QS)_3^{3-}$ at pH 7.3, $Zn(QS)_2^{2-}$ at pH 7.5 and $Cu(QS)_2^{2-}$ at pH 7.3. The black dotted line relates to the neat water|DCE interface. The initial concentrations in **Cell I** were (Al(III)-QS) [Al(III)] = 1.0×10^{-4} mol dm^{-3} and [QS] = 3.0×10^{-4} mol dm^{-3}, (Zn(II)-QS) [Zn(II)] = 1.0×10^{-4} mol dm^{-3} and [QS] = 2.0×10^{-4} mol dm^{-3}, (Cu(II)-QS) [Cu(II)] = 1.0×10^{-4} mol dm^{-3} and [QS] = 2.0×10^{-4} mol dm^{-3}, respectively.

The ion transfer and adsorption processes of the fluorescent Al(III) and Zn(II) complexes were further studied by PMF spectroscopy (cf. Supplementary material: **S4**). **Figures 4a** and **5** show the potential dependence of the PMF responses for $Al(QS)_3^{3-}$ and $Zn(QS)_2^{2-}$, respectively. In the Al(III)-QS system, the real (ΔF_{re}) and imaginary (ΔF_{im}) components of PMF were obtained as negative and positive signs at $\Delta_o^w\phi < -0.25$ V. The negative ΔF_{re} and positive ΔF_{im} signals for anionic species relate in principle to (i) quasi-reversible anion transfer across the interface and/or (ii) adsorption at the aqueous side of the interface. The PMF response associated with (i) quasi-reversible ion transfer (ΔF_t) is a linear function of the faradaic ac current ($i_{f,ac}$) [10].

$$\Delta F_t = \frac{4.606\varepsilon\Phi I_0}{j\omega zFS\cos\psi_i} i_{f,ac} \qquad (2)$$

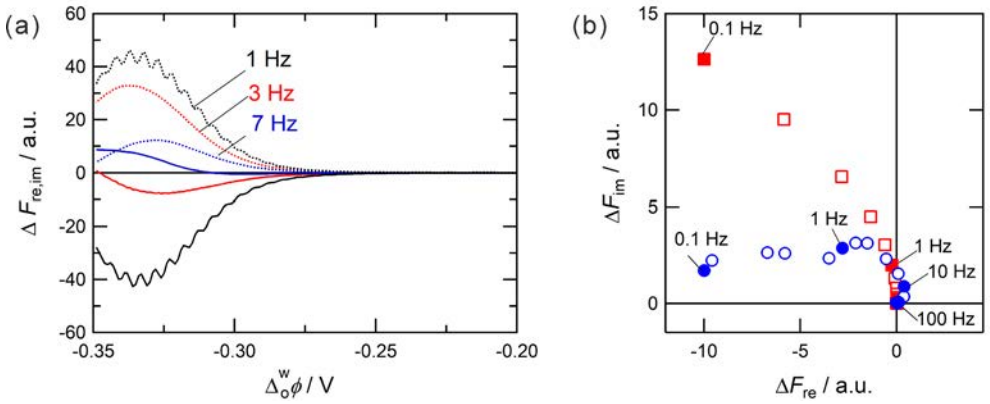

Figure 4. (a) Potential and (b) frequency dependences of the PMF responses for $Al(QS)_3^{3-}$ at pH 6.8. [Al(III)] = 3.0×10^{-4} mol dm^{-3} and [QS] = 9.0×10^{-4} mol dm^{-3} in **Cell II**. (a) The amplitude of potential modulation was 10 mV with a sweep rate of 5 mV s^{-1}. (b) The frequency response analyses were conducted at –0.30 V (blue) and –0.33 V (red), respectively, with an ac amplitude of 50 mV. The excitation and emission wavelengths were 404 nm and 508 nm, respectively.

where ε, Φ and I_0 are the molar absorption coefficient, the fluorescence quantum yield and the excitation photon flux, respectively. S is the interfacial area. The real and imaginary components of ΔF_t are expressed by

$$\Delta F_{t,re} = \frac{4.606\varepsilon\Phi I_0}{zFS\cos\psi_i}\left[\frac{\Delta_o^w\phi_{ac}\sigma\omega^{-3/2}}{(R_{ct}+\sigma\omega^{-1/2})^2+(\sigma\omega^{-1/2})^2}\right] \quad (3)$$

$$\Delta F_{t,im} = -\frac{4.606\varepsilon\Phi I_0}{zFS\cos\psi_i}\left[\frac{\Delta_o^w\phi_{ac}(R_{ct}+\sigma\omega^{-1/2})\omega^{-1}}{(R_{ct}+\sigma\omega^{-1/2})^2+(\sigma\omega^{-1/2})^2}\right] \quad (4)$$

where R_{ct} and σ are the charge transfer resistance, the Warburg term, respectively. In the latter case (ii), PMF associated with the adsorption from the aqueous side (ΔF_a^w) is proportional to the ac modulated surface coverage (θ_{ac}^w) [9].

$$\Delta F_a^w = 2.303\varepsilon\Phi I_0\Gamma_s^w S\theta_{ac}^w \quad (5)$$

$$\theta_{ac}^w = \frac{b^w zF}{RT}\left[\frac{\Delta_o^w\phi_{ac}(k_{a,dc}^w c_0^w\alpha^w(1-\theta_{dc}^w)-k_{d,dc}^w(\alpha^w-1)\theta_{dc}^w)}{k_{a,dc}^w c_0^w + k_{d,dc}^w + j\omega}\right] \quad (6)$$

where Γ_s^w, α, c_0^w and θ_{dc}^w are the saturated interfacial concentration, overall transfer coefficient for adsorption process, the bulk concentration and the dc surface coverage, respectively. $b^w\Delta_o^w\phi_{ac}$ is a portion of the Galvani potential difference for the adsorption process. $k_{a,dc}^w$ and $k_{d,dc}^w$ are the dc components of the adsorption and desorption rate constants at given potentials, respectively. The real and imaginary components of ΔF_a^w are represented by

$$\Delta F_{a,\,re}^{w} = \frac{2.303\varepsilon\,\Phi I_0\Gamma_s^w Sb^w zF}{RT}\left[\frac{\Delta_o^w\phi_{ac}(k_{a,dc}^w\,c_0^w\alpha^w(1-\theta_{dc}^w)-k_{d,dc}^w(\alpha^w-1)\theta_{dc}^w)\left(k_{a,dc}^w\,c_0^w+k_{d,dc}^w\right)}{k_{a,dc}^w\,c_0^w+k_{d,dc}^w+j\omega}\right] \tag{7}$$

$$\Delta F_{a,\,im}^{w} = -\frac{2.303\varepsilon\,\Phi I_0\Gamma_s^w Sb^w zF}{RT}\left[\frac{\Delta_o^w\phi_{ac}(k_{a,dc}^w\,c_0^w\alpha^w(1-\theta_{dc}^w)-k_{d,dc}^w(\alpha^w-1)\theta_{dc}^w)\omega}{k_{a,dc}^w\,c_0^w+k_{d,dc}^w+j\omega}\right] \tag{8}$$

Eqs. (3), (4) and (7), (8) indicate that ΔF_{re} and ΔF_{im} are negative and positive values for anionic species, respectively, for both (i) and (ii) cases. The complex plane plot, however, exhibits characteristic features for each process, i.e., (i) linear and (ii) semicircle responses [9]. The frequency response analysis of PMF was performed to elucidate the interfacial process of $Al(QS)_3^{3-}$ (**Figure 4b**). The PMF responses in a linear fashion was measured in the second quadrant ($\Delta F_{re} < 0$, $\Delta F_{im} > 0$) at −0.33 V, indicating the ion transfer process of anionic $Al(QS)_3^{3-}$ across the interface. At −0.30 V, the complex plane plot was expressed as a distorted semicircle in the second quadrant which associated with the adsorption process at the aqueous side of the interface. The distortion of the semicircle response at lower frequencies results from the overlapping of transfer signals [9].

In the Zn(II)-QS system, the PMF responses at pH 7.0 associate with the interfacial process of $Zn(QS)_2^{2-}$, in which the weak and intense PMF responses ($\Delta F_{re} < 0$, $\Delta F_{im} > 0$) were observed centered at −0.23 V and −0.34 V, respectively (**Figure 5**). The complex plane of the weak PMF response at −0.25 V exhibits a semicircle shape in the second quadrant (**Figure 5**, inset), indicating

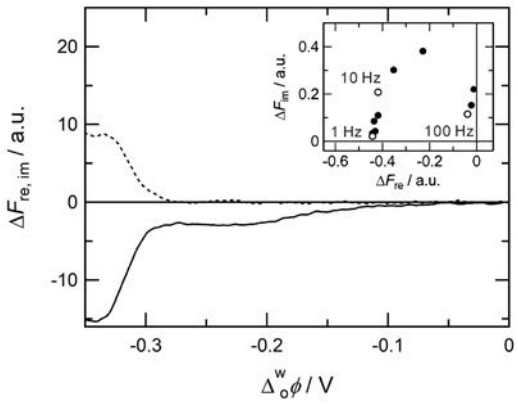

Figure 5. Potential and (inset) frequency dependences of the PMF responses for $Zn(QS)_2^{2-}$ at pH 7.0. The solid and dotted lines depict the real and imaginary components, respectively. The potential modulation was 30 mV at 1 Hz with a sweep rate of 2 mV s^{-1}. The frequency response analysis was conducted at −0.25 V with an ac amplitude of 20 mV. [Zn(II)] = 5.0×10^{-5} mol dm^{-3} and [QS] = 1.0×10^{-4} mol dm^{-3} in **Cell II**. The excitation and emission wavelengths were 404 nm and 525 nm, respectively.

the adsorption process of $Zn(QS)_2^{2-}$ at the aqueous side of the interface. The intense PMF response around −0.34 V could be attributed to the ion transfer of $Zn(QS)_2^{2-}$, which is supported by the significant increase in the total fluorescence intensity from the interfacial region as discussed in Section 3.2. In addition, the PMF intensity for the adsorption of $Zn(QS)_2^{2-}$ at $-0.30\ \text{V} < \Delta^{w}_{o}\phi < -0.20\ \text{V}$ was varied with the light-polarization of the incident beam, where the larger PMF signals were measured by the s-polarized incident beam (Supplementary material: **S5**). The light-polarization dependence of PMF relates to the molecular orientation of the fluorescent species adsorbed at the interface [33]. The adsorption state of the QS complex including molecular orientation is discussed in detail through the PM-TIRF analysis in Section 3.2.

3.2. Characterization of adsorption species at the water|DCE interface

The effects of pH and potential on the adsorption state of the interfacial species were studied in the Al(III)-QS systems at pH 7.0 and 4.9 through the PM-TIRF analysis. The dominant species in the aqueous phase is $Al(QS)_3^{3-}$ at pH 7.0 ($Al(QS)_3^{3-}$:$Al(QS)_2^-$ = 86:8), whereas $Al(QS)_2^-$ is the major species at pH 4.9 ($Al(QS)_3^{3-}$: $Al(QS)_2^-$: $Al(QS)^+$ = 6 : 59 : 28). **Figure 6** shows the potential dependences of the PM-TIRF response ($\Delta F^{p\text{-}s}$) measured in the Al(III)-QS system. The negative $\Delta F^{p\text{-}s}$ magnitude was maximized around at −0.33 V, where the intense PMF response was observed (cf. **Figure 3a**). The $\Delta F^{p\text{-}s}$ signal was steeply weakened at $\Delta_o^w\phi < -0.33$ V, and the synchronous enhancement of F_{total}, which is mainly associated with increase of fluorescent species in DCE, indicated the ion transfer of Al(III)-QS complex. In the Al(III)-QS system, the fluorescence signal arisen from the centrosymmetric $Al(QS)_3^{3-}$ molecule is not affected by the modulation of the linear light-polarization even if $Al(QS)_3^{3-}$ is adsorbed at the interface. Therefore, the non-zero $\Delta F^{p\text{-}s}$ signals relate to the adsorption process of the square-planar 1:2 complex ($Al(QS)_2^-$) at the interface although the abundance of $Al(QS)_2^-$ is rather small, ~8%. Considering the planar $Al(QS)_2^-$ with the excitation dipole moment in quinoline ring, the average orientation angle (θ_{OR}) of $Al(QS)_2^-$ can be estimated from $\Delta F^{p\text{-}s}$ and F_{total} [11]. The θ_{OR} value at $-0.25\text{ V} < \Delta_o^w\phi < -0.20$ V was approximately constant at 63±2° (Supplementary material: **S6)**. The magnitude of negative $\Delta F^{p\text{-}s}$ signals was relatively increased at pH 4.9, where the orientation angle was determined as $\theta_{OR} = 67 \pm 3°$ at $-0.25\text{ V} < \Delta_o^w\phi < -0.20$ V.

In order to further characterize the interfacial species, the wavelength-dependence of $\Delta F^{p\text{-}s}$, i.e. PM-TIRF spectrum, was measured at given potentials. The PM-TIRF spectrum corresponds to fluorescence spectrum of the interfacial species oriented at the interface. Undesirable Raman scattering from the water-saturated DCE phase on the optical path was subtracted in the PM-TIRF

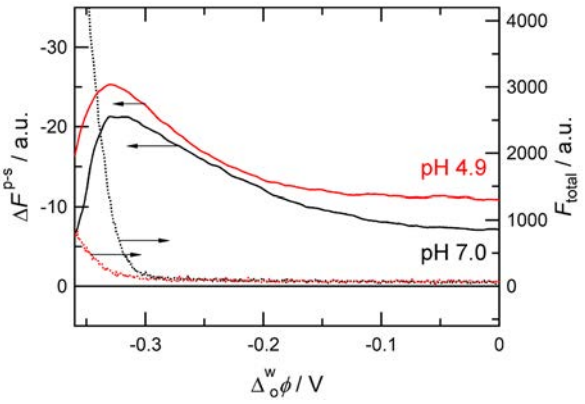

Figure 6. Potential dependence of $\Delta F^{p\text{-}s}$ and F_{total} for the Al(III)-QS complex systems at pH 7.0 (black) and 4.9 (red). The potential sweep rate was 2 mV s^{-1}. The excitation and emission wavelengths were 376 nm and 492 nm, respectively. The concentrations in **Cell II** were (pH 7.0) [Al(III)] = 1.0×10^{-4} mol dm^{-3} and [QS] = 3.0×10^{-4} mol dm^{-3}, and (pH 4.9) [Al(III)] = 1.0×10^{-4} mol dm^{-3}, [QS] = 2.0×10^{-4} mol dm^{-3}, respectively.

spectra (Supplementary material: **S6**). The baseline subtracted PM-TIRF spectra for Al(III)-QS complexes are shown in **Figure 7**. The maximum wavelengths (λ_{max}) of the PM-TIRF spectra are summarized in **Table 1**. The PM-TIRF maximum at pH 7.0 was found around 496 nm. The spectral features were similar to those measured in the aqueous solution at pH 4.9 where the major species is $Al(QS)_2^-$. These results exhibited that $Al(QS)_2^-$ adsorbed at the interface is detectable with a high selectivity in the PM-TIRF measurement. It should be noted that $Al(QS)_3^{3-}$ would also be adsorbed at the interface, but the spherical $Al(QS)_3^{3-}$ molecule is not responsible for PM-TIRF signal. At pH 4.9, the PM-TIRF maximum was red-shifted from 496 nm for the bulk aqueous species to >501 nm. Since the adsorption of the cationic 1:1 complex, $Al(QS)^+$, which is one of the minor aqueous species (28%), occurred hardly in the negative potential region, the observed red-shift of PM-TIRF spectra could be related to the π-π stacking of QS ligands of $Al(QS)_2^-$ at the interface [34-36].

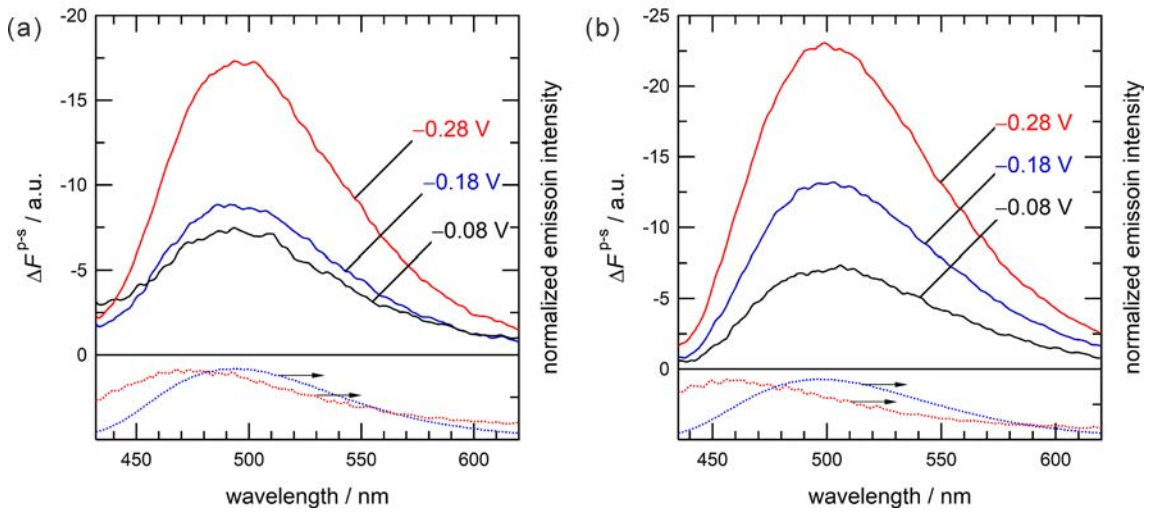

Figure 7. PM-TIRF spectra for Al(III)-QS complexes at (a) pH 7.0 and (b) 4.9 at the water|DCE interface. The blue and red dashed lines refer to normalized fluorescence spectra measured in the aqueous and organic solutions. The excitation wavelength were 376 nm. The concentrations in **Cell II** were (a) [Al(III)] = 1.0×10^{-4} mol dm^{-3} and [QS] = 3.0×10^{-4} mol dm^{-3}, and (b) [Al(III)] = 1.0×10^{-4} mol dm^{-3} and [QS] = 2.0×10^{-4} mol dm^{-3}, respectively.

Table 1. PM-TIRF maxima (λ_{max}) of Al(III)-QS complexes at the water|DCE interface.

	pH 4.9		pH 7.0	
	$\Delta_o^w\phi$ / V	λ_{max} / nm	$\Delta_o^w\phi$ / V	λ_{max} / nm
interface	−0.11	503	−0.08	494
	−0.21	503	−0.18	496
	−0.31	501	−0.28	496
aqueous phase[a]		496		493
organic phase[a]		456		478

[a]The fluorescence maximum wavelengths in the aqueous and organic phases.

In the case of the Zn(II)-QS system, the negative $\Delta F^{p\text{-}s}$ signals in the negative potential region were observed at different pHs, where the major species in the aqueous phase were the anionic $Zn(QS)_2^{2-}$ at pH 7.0 and neutral Zn(QS) at pH 6.1, respectively (**Figure 8a**, see also Supplementary material: **S2**). The $\Delta F^{p\text{-}s}$ intensity was dependent on $\Delta_o^w\phi$ at both pHs indicating

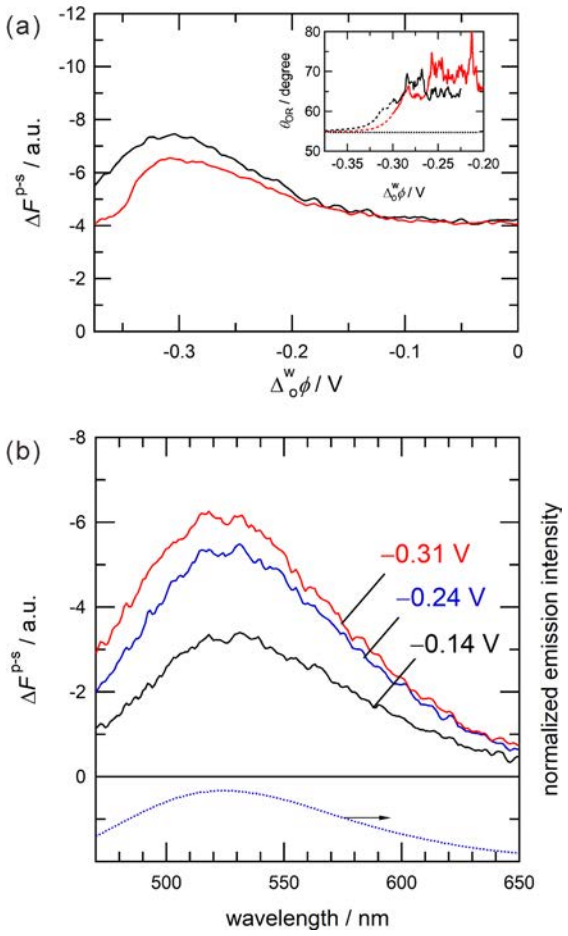

Figure 8. Potential dependence of (a) PM-TIRF signals at 525 nm and (b) PM-TIRF spectra at pH 7.0 for the Zn(II)-QS system. (a) The red and black lines were measured at pH 6.1 and 7.0, respectively. The potential sweep rate was 2 mV s^{-1}. (Inset) θ_{OR} vs. $\Delta^{w}_{o}\phi$ plots. (b) The blue dotted line refers to normalized fluorescence spectra measured in aqueous solution. The excitation wavelength was 404 nm. [Zn(II)] = 5.0×10^{-5} mol dm^{-3} and [QS] = 1.0×10^{-4} mol dm^{-3} in **Cell II**.

that the $\Delta F^{p\text{-}s}$ responses originate from $Zn(QS)_2^{2-}$ adsorbed at the interface. In a similar manner to $Al(QS)_2^{-}$, the average orientation angles of the excitation dipole of $Zn(QS)_2^{2-}$ at $-0.25\ V < \Delta^{w}_{o}\phi < -0.20\ V$ were determined as 65±2° at pH 7.0 and 70±2° at pH 6.1, respectively (**Figure 8a**, inset). The negative $\Delta F^{p\text{-}s}$ signals were maximized around −0.31 V, which is lightly less negative

potential than −0.34 V of the ion transfer of $Zn(QS)_2^{2-}$ observed in the PMF experiments. The $\Delta F^{p\text{-}s}$ intensity was weakened after the ion transfer of $Zn(QS)_2^{2-}$. The PM-TIRF spectra of Zn(II)-QS complexes at pH 7.0 are shown in **Figure 8b** (cf. **Table 2**). The spectral characteristics of PM-TIRF spectra were not significantly affected by the potential, but the PM-TIRF intensity was enhanced at −0.31 V. The PM-TIRF spectra at pH 6.1 were analogous to those measured at pH 7.0 (Supplementary material: **S6**). The contribution from the neutral 1:1 complex, Zn(QS), was not quantitatively-assessed because of similar spectral features between Zn(QS) and $Zn(QS)_2^{2-}$ [37]. The potential-dependent PM-TIRF responses, however, indicate that the charged $Zn(QS)_2^{2-}$ is adsorbed with a hydration state similar to the aqueous species.

Table 2. PM-TIRF maxima (λ_{max}) of Zn(II) complexes at the water|DCE interface.

	$Zn(QS)_2^{2-}$		$Zn(QC)_2^{2-}$	
	$\Delta_o^w\phi$ / V	λ_{max} / nm	$\Delta_o^w\phi$ / V	λ_{max} / nm
interface			−0.08	584
	−0.14	526	−0.18	584
	−0.24	524	−0.28	584
	−0.31	522	−0.33	567
aqueous phase[a]		523		645
organic phase[a]		–		562

[a]The fluorescence maximum wavelengths in the aqueous and organic phases.

The interfacial behavior of the Zn(II)-QC complex was examined as a control system to assess the influence of coordination geometry. The free QC ligand with pK_{a1} = 3.94 and pK_{a2} = 9.98 exists as HQC^- around pH 7 and the complexation with Zn(II) takes place quantitatively [38]. The major species of the Zn(II)-QC system under neutral and alkaline conditions is a divalent 1:2 complex, $Zn(QC)_2^{2-}$, of which two tridentate QC ligands occupy six coordination sites of the zinc center. In the capacitance curves, $Zn(QC)_2^{2-}$ exhibited a significant adsorption at $-0.20\ V < \Delta_o^w\phi <$

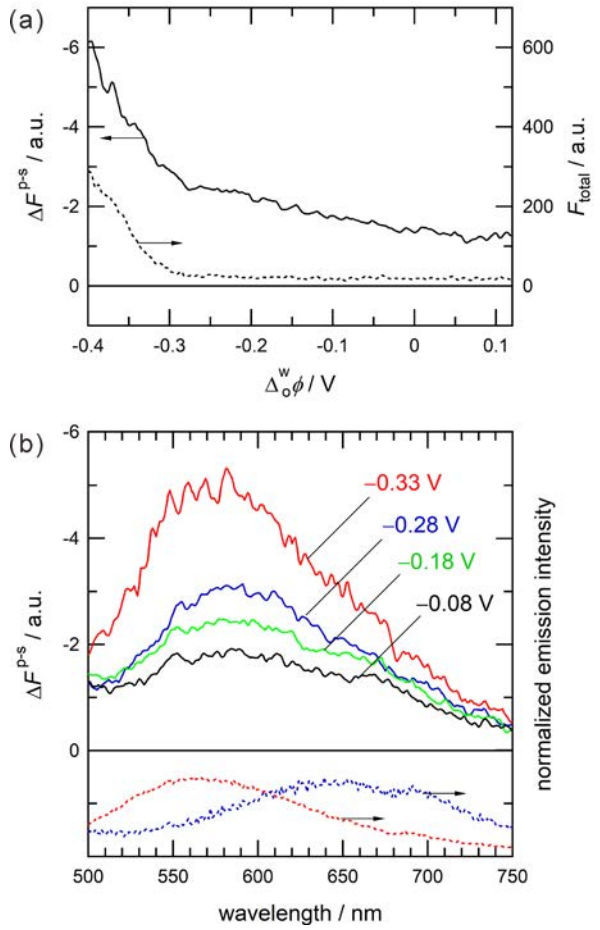

Figure 9. The potential dependences of (a) PM-TIRF signals at 590 nm and (b) PM-TIRF spectra measured for $Zn(QC)_2^{2-}$ at pH 7.5. (a) The potential sweep rate was 2 mV s^{-1}. The excitation wavelength was 404 nm. [Zn(II)] = [QC] = 1.0×10^{-4} mol dm^{-3} in **Cell II**. (b) The blue and red dotted lines refer to normalized fluorescence spectra measured in the aqueous and organic solutions.

0.10 V, whereas only the slight adsorption responses were observed in the PMF measurement (see Supplementary material: **S7**). The PMF response is rather weakened for "strong" adsorption process because of an irreversible ac potential-dependence. The similar signal lowering of the adsorption response has been reported in the protoporphyrin IX system with the high surface activity at the water|DCE interface [39]. In contrast to the PMF response, the intense ΔF^{p-s} signals

were observed for $Zn(QC)_2^{2-}$ as shown in **Figure 9a**, in which the negative $\Delta F^{p\text{-}s}$ magnitude increased synchronously with increasing F_{total} at $\Delta_o^w\phi < -0.30$ V. The PM-TIRF maxima at $\Delta_o^w\phi > -0.33$ V showed intermediate λ_{max} values between the fluorescence maxima in the bulk aqueous (645 nm) and organic phases (562 nm) (**Figure 9b** and **Table 2**), while the spectral feature at −0.33 V was close to that of the organic species. These PM-TIRF results manifest the adsorption state of $Zn(QC)_2^{2-}$ modified at the interface depending on $\Delta_o^w\phi$, and the spectral shifts could reflect the specific polarity of adsorption plane in the interfacial region. Considering no clear spectral shift for $Zn(QS)_2^{2-}$ approximately identical to the aqueous species with axial hydration (**Figure 8b**), these contrastive PM-TIRF results indicate that the adsorption state of metal complexes is highly affected by the coordination geometry.

4. Conclusions

The present results for the water-soluble 8-quinolinol compound demonstrated that the interfacial mechanism and adsorption state were affected by metal center, charged state, coordination geometry, and so on. The PMF and PM-TIRF studies achieved the mechanistic analysis of the potential-driven process as well as the direct characterization of the adsorption state of the fluorescent Al(III) and Zn(II) complexes. The PMF analysis elucidated these anionic complexes were transferred across the interface accompanied by the adsorption at the aqueous side of the interface. In addition, the adsorption state and molecular orientation of the square-planar 1:2 complexes, $Al(QS)_2^-$ and $Zn(QS)_2^{2-}$, were analyzed with high selectivity by PM-TIRF spectroscopy. The interfacial species of the 1:2 complexes were analogous to the aqueous species with axial hydration. In the Zn(II) complex system, the effect of coordination geometry on the adsorption state was highlighted by comparing the bidentate QS ligand with the tridentate QC. The

spectroelectrochemical results indicated a relatively strong interfacial adsorption of $Zn(QC)_2^{2-}$ with the intermediate state between the aqueous and organic species. These results suggest that the hydration and solvation of the interfacial species play a crucial role in the adsorption behavior of metal complexes. The present experimental approach will provide insights into the developments in separation science with functional ligands and heterogeneous reaction system where metal complexes with specific orientation at the interface form self-assembled layers or highly ordered supramolecular structures.

Acknowledgements

This work was supported by Grants-in-Aid for Scientific Research (C) (Nos.19K05541 and 16K05811)) from Japan Society for the Promotion of Science (JSPS) and the Kanazawa University CHOZEN Project. S. Y. thanks the JSPS Research Fellowship for Young Scientists (No.17J02009).

References

[1] I. Benjamin, Reaction dynamics at liquid interfaces, Annu. Rev. Phys. Chem. 66 (2015) 165-188.

[2] I. Benjamin, Static and dynamic electronic spectroscopy at liquid interfaces, Chem. Rev. 106(4) (2006) 1212-1233.

[3] H. Nagatani, *In situ* spectroscopic characterization of porphyrins at liquid interfaces, in: K.M. Kadish, K.M. Smith, R. Guilard (Eds.), Handbook of Porphyrin Science, World Scientific Publishing Co., Singapore, 2014, pp. 51-96.

[4] J.M. Perera, G.W. Stevens, Spectroscopic studies of molecular interaction at the liquid-liquid interface, Anal. Bioanal. Chem. 395(4) (2009) 1019-1032.

[5] S. Amemiya, A.J. Bard, F.R.F. Fan, M.V. Mirkin, P.R. Unwin, Scanning electrochemical microscopy, Annu. Rev. Anal. Chem. 1 (2008) 95-131 031207.112938.

[6] H.H. Girault, Electrochemistry at liquid-liquid interfaces, in: A.J. Bard, C.G. Zoski (Eds.), Electroanalytical Chemistry, CRC Press, 2010, pp. 1-104.

[7] Z. Yoshida, Electrochemical study of solvent extraction based on ion transfer at the aqueous/organic solution interface, Solvent Extr. Res. Dev., Jpn. 18 (2011) 15-35.

[8] Z. Samec, Electrochemistry at the Interface between Two Immiscible Electolyte Solutions, Pure Appl. Chem. 76(12) (2004) 2147-2180.

[9] H. Nagatani, D.J. Fermín, H.H. Girault, A kinetic model for adsorption and transfer of ionic species at polarized liquid|liquid interfaces as studied by potential modulated fluorescence spectroscopy, J. Phys. Chem. B 105(39) (2001) 9463-9473.

[10] H. Nagatani, T. Sagara, Potential-modulation spectroscopy at solid/liquid and liquid/liquid interfaces, Anal. Sci. 23(9) (2007) 1041-1048.

[11] S. Yamamoto, H. Nagatani, K. Morita, H. Imura, Potential-dependent adsorption and orientation of *meso*-substituted porphyrins at liquid|liquid interfaces studied by polarization-modulation total internal reflection fluorescence spectroscopy, J. Phys. Chem. C 120(13) (2016) 7248-7255.

[12] S. Yamamoto, H. Nagatani, H. Imura, Potential-induced aggregation of anionic porphyrins at liquid|liquid interfaces, Langmuir 33(39) (2017) 10134-10142.

[13] J.P. Phillips, The reactions of 8-quinolinol, Chem. Rev. 56(2) (1956) 271-297.

[14] H.D. Burrows, T. Costa, M.L. Ramos, A.J.M. Valente, B. Stewart, L.L.G. Justino, A.I.A. Almeida, N.L. Catarina, R. Mallavia, M. Knaapila, Self-assembled systems of water soluble metal

8-hydroxyquinolates with surfactants and conjugated polyelectrolytes, Phys. Chem. Chem. Phys. 18(25) (2016) 16629-16640.

[15] S. Li, J. Lu, H. Ma, D. Yan, Z. Li, S. Qin, D.G. Evans, X. Duan, Luminous ultrathin films by the ordered micellar assembly of neutral bis(8-hydroxyquinolate)zinc with layered double hydroxides, J. Phys. Chem. C 116(23) (2012) 12836-12843.

[16] S. Sawada, T. Osakai, Mechanism of electrochemical solvent extraction of divalent metal ions with quinolin-8-ol, Analyst 122(12) (1997) 1597-1600.

[17] M. Itagaki, T. Ono, K. Watanabe, Application of electrochemical impedance spectroscopy to solvent extraction of metallic ions, Electrochim. Acta 44(24) (1999) 4365-4371.

[18] M. Itagaki, H. Fukushima, K. Watanabe, Studies on electrochemical solvent extraction of metal ions at water/1,2-dichloroethane interface, Anal. Sci. 17(7) (2001) 819-824.

[19] A. Mastouri, S. Peulon, N. Bellakhal, A. Chaussé, M(II) transfer across a liquid-liquid microinterface facilitated by a complex formation with 8-Hydroxyquinoline: Application to quantification of Pb(II), Cd(II) and Zn(II) alone or in mixture in effluents, Electrochim. Acta 130 (2014) 818-825.

[20] A.I. Azcurra, L.M. Yudi, A.M. Baruzzi, Interfacial phenomena involving Fe(III)-ofloxacin complexes at the water|1,2-dichloroethane interface, J. Electroanal. Chem. 461(1-2) (1999) 194-200.

[21] A.I. Azcurra, L.M. Yudi, A.M. Baruzzi, Interaction of ofloxacin-Al(III) pH dependent complexes with the water|1,2-dichloroethane interface, J. Electroanal. Chem. 560(1) (2003) 35-42.

[22] T. Wandlowski, V. Marecek, Z. Samec, Galvani potential scales for water-nitrobenzene and water-1,2-dichloroethane interfaces, Electrochim. Acta 35(7) (1990) 1173-1175.

[23] V. Gobry, S. Ulmeanu, F. Reymond, G. Bouchard, P.-A. Carrupt, B. Testa, H.H. Girault, Generalization of ionic partition diagrams to lipophilic compounds and to biphasic systems with variable phase volume ratios, J. Am. Chem. Soc. 123(43) (2001) 10684-10690.

[24] F. Reymond, G. Steyaert, P.A. Carrupt, B. Testa, H. Girault, Ionic partition diagrams: A potential-pH representation, J. Am. Chem. Soc. 118(47) (1996) 11951-11957.

[25] H. Sakae, H. Nagatani, H. Imura, Ion transfer and adsorption behavior of ionizable drugs affected by PAMAM dendrimers at the water|1,2-dichloroethane interface, Electrochim. Acta 191 (2016) 631-639.

[26] J. Fresco, H. Freiser, Stabilities of chelates of certain substituted 8-quinolinols, Inorg. Chem. 2(1) (1963) 82-85.

[27] D. Badocco, A. Dean, V. Di Marco, P. Pastore, Electrochemical characterization of 8-hydroxyquinoline-5-sulphonate/aluminium(III) aqueous solutions, Electrochim. Acta 52(28) (2007) 7920-7926.

[28] J.L. Beltrán, R. Codony, M.D. Prat, Evaluation of stability constants from multi-wavelength absorbance data: program STAR, Anal. Chim. Acta 276(2) (1993) 441-454.

[29] V. Pacáková, P. Coufal, K. Štulík, Capillary electrophoresis of inorganic cations, J. Chromatogr. A 834(1) (1999) 257-275.

[30] M. Luisa Ramos, L.L.G. Justino, A. Branco, C.M.G. Duarte, P.E. Abreu, S.M. Fonseca, H.D. Burrows, NMR, DFT and luminescence studies of the complexation of Zn(II) with 8-hydroxyquinoline-5-sulfonate, Dalton Trans. 40(44) (2011) 11732-11741.

[31] M. Albrecht, K. Witt, P. Weis, E. Wegelius, R. Fröhlich, Zinc(II) complexes of amide- and urea-substituted 8-hydroxyquinolines, Inorg. Chim. Acta 341 (2002) 25-32.

[32] A.K. Das, Studies on mixed ligand complexes of cobalt(II), nickel(II), copper(II) and zinc(II) involving 8-hydroxyquinoline-5-sulphonic acid as a primary ligand and substituted catechols as secondary ligands, Transition Met. Chem. 14(3) (1989) 200-202.

[33] H. Nagatani, R.A. Iglesias, D.J. Fermín, P.F. Brevet, H.H. Girault, Adsorption behavior of charged zinc porphyrins at the water/1,2-dichloroethane interface studied by potential modulated fluorescence spectroscopy, J. Phys. Chem. B 104(29) (2000) 6869-6876.

[34] M. Brinkmann, G. Gadret, M. Muccini, C. Taliani, N. Masciocchi, A. Sironi, Correlation between molecular packing and optical properties in different crystalline polymorphs and amorphous thin films of *mer*-tris(8-hydroxyquinoline)aluminum(iii), J. Am. Chem. Soc. 122(21) (2000) 5147-5157.

[35] H.-L. Gao, S.-X. Jiang, Y.-M. Hu, F.-F. Li, Q.-Q. Zhang, X.-Y. Shi, J.-Z. Cui, Syntheses, structures and luminescent properties of the metal complexes based on Zn(II) or Cd(II) with 5-nitro-8-hydroxyquinoline, Inorg. Chem. Commun. 44 (2014) 58-62.

[36] L.S. Sapochak, F.E. Benincasa, R.S. Schofield, J.L. Baker, K.K.C. Riccio, D. Fogarty, H. Kohlmann, K.F. Ferris, P.E. Burrows, Electroluminescent zinc(II) bis(8-hydroxyquinoline): Structural effects on electronic states and device performance, J. Am. Chem. Soc. 124(21) (2002) 6119-6125.

[37] R. van Slageren, G. den Boef, W.E. van der Linden, Determination of traces of zinc by fluorimetrically indicated complexometric titrations, Talanta 20(8) (1973) 739-748.

[38] F.C. McDonald, R.C. Applefield, C.J. Halkides, J.H. Reibenspies, R.D. Hancock, A thermodynamic and crystallographic study of complexes of the highly preorganized ligand 8-hydroxyquinoline-2-carboxylic acid, Inorg. Chim. Acta 361(7) (2008) 1937-1946.

[39] H. Nagatani, T. Ozeki, T. Osakai, Direct spectroelectrochemical observation of interfacial species at the polarized water/1,2-dichloroethane interface by ac potential modulation technique, J. Electroanal. Chem. 588(1) (2006) 99-105.

Graphical Abstract